Theoretical study of magnetic properties and x-ray magnetic circular dichroism of the ordered $Fe_{0.5}Pd_{0.5}$ alloy

I. Galanakis, S. Ostanin, M. Alouani, and H. Dreyssé
Institut de Physique et de Chimie des Matériaux de Strasbourg (IPCMS), 23 rue du Loess, 67037 Strasbourg Cedex, France

J. M. Wills
Center for Materials Science and Theoretical Division, Los Alamos National Laboratory, Los Alamos, New Mexico 87544
(Received 17 May 1999; revised manuscript received 4 August 1999)

A detailed theoretical study of magnetic and structural properties of $Fe_{0.5}Pd_{0.5}$ ordered face-centered tetragonal (fct) alloy, using both the local spin density approximation (LSDA) and the generalized gradient approximation (GGA), is presented. The total energy surface as a function of the lattice parameters *a* and *c* shows a long valley where stable structures may exist. Our calculation using the GGA predicts a magnetic phase transition from perpendicular to parallel magnetization as a function of the lattice parameter, whereas LSDA favors always the [001] magnetization axis for all values of the lattice parameters. The spin and orbital magnetic moments and x-ray magnetic circular dichroism spectra are calculated for the easy [001] and the hard [100] magnetization axis and for three sets of experimental lattice parameters, and are compared to the available experimental results on these films. A supercell calculation for a 4 monolayer $Fe_{0.5}Pd_{0.5}$ thin film produced similar results. While the spin magnetic moments are in fair agreement with experiment, the orbital magnetic moments are considerably underestimated. To improve the agreement with experiment we included an atomic orbital polarization term; however, the computed orbital moments scarcely changed.

I. INTRODUCTION

Magnetic films with strong perpendicular magnetization anisotropy (PMA) are greatly attractive and promising for magneto-optical recording devices. Recently, a number of chemically ordered binary *d*-metal layered systems with perpendicular magnetization have been elaborated.[1] This direction of the magnetization is due to the bulk magnetocrystalline anisotropy energy (MCA). The chemical ordering in these films normally is accompanied by an increased Kerr rotation.[2,3]

$Fe_{0.5}Pd_{0.5}$ alloy as bulk or film has been extensively studied in recent years.[4] The bulk alloy at low temperature adopts a disordered γ phase with fcc lattice and lattice parameter $a=3.8$ Å.[5] At 920 K, it exhibits a phase transition towards an ordered face-centered tetragonal (fct) structure. This structure is ferromagnetic because the $L1_0$ intermetalic phase is characterized by a high uniaxial MCA.[6] Recently, it was made possible by molecular beam epitaxy (MBE) the production of films of this alloy presenting the $L1_0$ structure due to the constraints imposed by the substrates.[7–9] These films present different lattice parameters depending on the preparation conditions and the growth temperature.

The spin-dependent electronic structure of the $Fe_{0.5}Pd_{0.5}$ alloy remains under consideration. Previous first-principles band calculations of $Fe_{0.5}Pd_{0.5}$ alloy have been performed for the CuAu (pseudocubic) crystalline structure.[10–12] The MCA and the anisotropy of the orbital angular momentum have been investigated theoretically by means of a perturbative technique for the spin-orbit interaction.[10,12]

It has been recently demonstrated by Weller *et al.*[13] that x-ray magnetic circular dichroism (XMCD) is also a suitable technique to probe MCA at an atomic scale, via the determination of the anisotropy of the orbital magnetic moment on a specific shell and site. This is because XMCD spectroscopy uses circularly polarized radiation to probe element specific magnetic properties of alloys.[14] Although x-ray absorption spectroscopy (XAS) probes unoccupied states above the Fermi energy, the XMCD sum rules[15–17] allow the determination of the spin and orbital magnetic moments of the absorptive atom. However their application to itinerant systems, in particular to low symmetry systems, is debated since these sum rules are derived from atomic theory. [16,18,19] Nevertheless, the difference of the XMCD signal for different magnetization axis could be directly related to the MCA.

The theoretical understanding of XMCD of magnetic material is not an easy task, and several *ab initio* calculations have attempted to compute the XMCD of transition metals and rare earth compounds.[20–25] The L_2 and L_3 edges involving electronic excitations of $2p$-core electrons towards *d*-conduction states have attracted much attention due to the dependence of the dichroic signal on the exchange-splitting and the spin-orbit coupling of both initial core and final valence states. Wu *et al.* used the slab linear augmented plane wave method to study the $L_{2,3}$ XMCD of Fe but unfortunately they did not compare their data to experimental results.[20] Brouder and co-workers,[23] Guo,[24] and Ankudinov and Rehr[25] used multiple scattering theory to study XMCD but their method, although successful, has only been applied to systems with few atoms per unit cell. This is because multiple scattering methods, which are usually carried out in real space using large clusters, are very expensive on CPU and require a large processor memory. Finally, atomic calculations, using crystal field symmetry, are widely applied to fit the experimental $M_{4,5}$ edges of rare earths and actinide compounds and the $L_{2,3}$ edges of early transition metals. How-

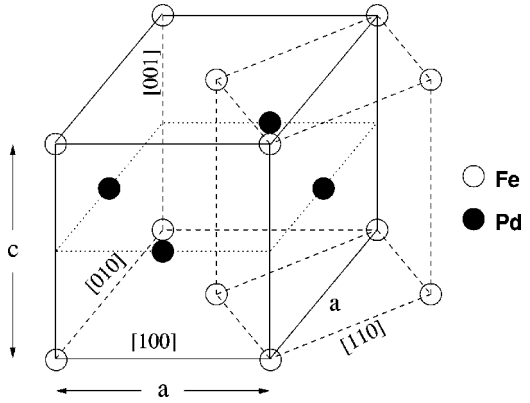

FIG. 1. $Fe_{0.5}Pd_{0.5}$ ordered fct alloy can be seen as a system of alternating Fe and Pd layers. The unit cell used in the calculations is also presented.

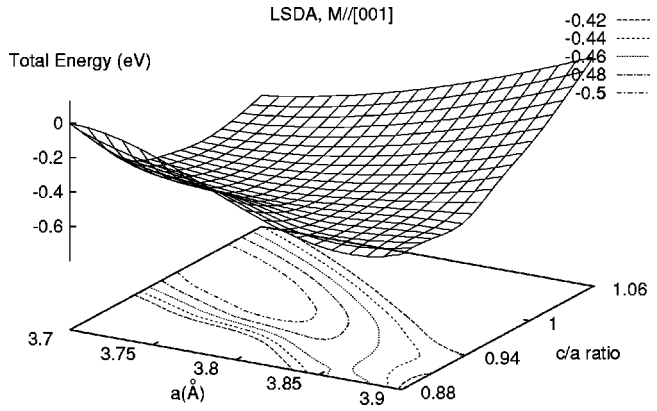

FIG. 2. Total energy surface within LSDA and for magnetization axis along the [001] direction as a function of the lattice parameter a and the c/a ratio. The energy step between two contours is 0.02 eV. We observe the existence of a valley along an isovolume line which could lead to the possibility of finding stable structures inside this valley. Such structures could exist due to lattice mismatch between the $Fe_{0.5}Pd_{0.5}$ and a substrate combined with the temperature effect. The global minimum corresponds to $a = 3.732$ Å and $c/a = 0.984$.

ever, because of the large number of parameters to fit, it is difficult to apply this formalism to delocalized $3d$ states.[26]

In this work we use the relativistic full-potential linear muffin-tin orbital method (FP-LMTO) (Ref. 27) to compute the structural, electronic, and magnetic properties of $Fe_{0.5}Pd_{0.5}$ and calculate XMCD spectra and compare our results with experiment. In the second section we investigate the ground state and explain qualitatively the stable experimental fct structures for a wide range of lattice parameters when grown over different substrates. A supercell calculation for a 4 monolayer (ML) thin film is presented. In Sec. III we present the magnetic properties of $Fe_{0.5}Pd_{0.5}$. Finally in the fourth section of this paper we use our method[22] to compute the XMCD spectra for different exchange-correlation potentials and for some selected sets of lattice parameters and compare our results to experiment.

II. STRUCTURAL PROPERTIES

In this section we discuss the structural properties of $Fe_{0.5}Pd_{0.5}$ system with respect to the magnetization axis. The unit cell contains one atom of Pd and one of Fe and is presented in Fig. 1. Experimentally, films of different lattice constants of this material have been synthesized, and it was found that the measured magnetic properties are different highlighting the importance of the lattice mismatch between the sample and the substrate.[7–9] Previous calculations showed that the results for these properties depend strongly on the type of exchange-correlation potential used to solve Kohn-Sham equations.[28] In this work, we use both the local-spin density approximation (LSDA) (Ref. 29) and the generalized gradient approximation (GGA).[30]

Figures 2 and 3 show our calculated total-energy surfaces of $Fe_{0.5}Pd_{0.5}$ with respect to the value of the lattice parameter a and the c/a ratio within LSDA for the magnetization axis along the [001] and [100] directions, respectively. Both graphs show the same characteristics, in particular, an anharmonic valley that follows practically an isovolume line. The total minimum corresponds to the same lattice parameters for both surfaces ($a = 3.732$ and $c/a = 0.984$). The total energy surface for $\mathbf{M}\|[100]$ lies just above that for $\mathbf{M}\|[001]$. The energy difference between the two magnetization axis and for any set of lattice parameters lies in the range [8 meV, 14 meV]. For the global minimum the energy difference is 11.84 meV. LSDA favors the [001] magnetization axis and gives no magnetic phase transition as a function of the a and c lattice parameters.

Figures 4 and 5 show similar total energy surfaces, calculated by using the GGA to the exchange-correlation potential.[30] It is interesting to notice that the GGA surfaces show a different behavior than these calculated within the LSDA. We observe also a similar valley to the one produced within the LSDA but it is shifted towards higher c/a values in agreement with experiment. This shift is expected since LSDA is well known to overbind. The minimum of the total energy is shallower than the one produced within LSDA. This result is also not surprising because of the overbinding nature of LSDA resulting on higher bulk modulus. So as expected GGA reduced the bulk modulus from its LSDA value. The very smooth nature of the bottom of the valley makes it possible for the system to easily change the a and

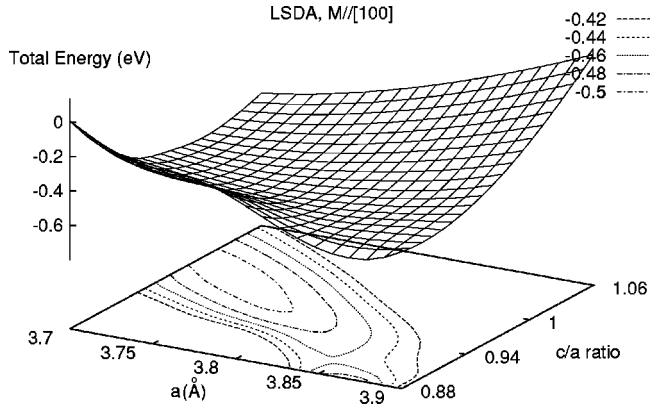

FIG. 3. The same as Fig. 2 but for $\mathbf{M}\|[100]$ direction. The surface has exactly the same form as for $\mathbf{M}\|[001]$ but lays just above this surface, so that LSDA favors always the [001] axis in the range of the studied lattice parameters. Both surfaces have the minimum for the same lattice parameters ($a = 3.732$ Å and $c/a = 0.984$). The two global minima are separated by 11.84 meV.

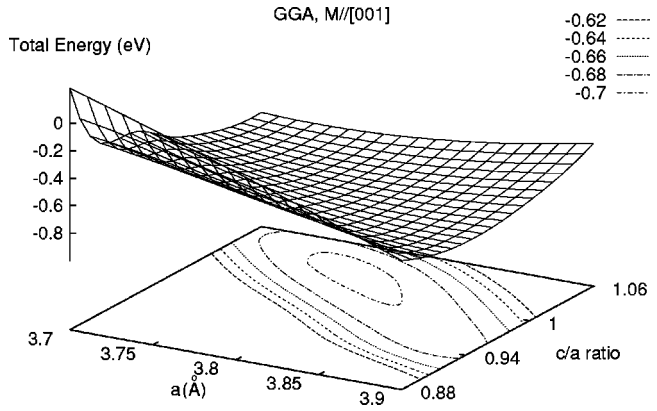

FIG. 4. The same as Fig. 2 but the calculations are within the GGA. The surface shows the same structure as that of LSDA, but the valley is shifted towards higher c/a ratios. This valley passes through all experimental lattice parameters points. The large difference between LSDA and GGA energy surface shows that for $Fe_{0.5}Pd_{0.5}$ the results depend strongly on the type of the exchange-correlation potential used. The global minimum corresponds to the point $a=3.774$ Å and $c/a=1.022$.

c/a ratio by applying some external constraint and remains stable as long as these parameters are located on the total energy valley. The external constraint could arise from a lattice mismatch between $Fe_{0.5}Pd_{0.5}$ and the substrate, which is the case of the samples discussed below. For $\mathbf{M}\|[001]$ the global minimum corresponds to $a=3.774$ and $c/a=1.022$, whereas for $\mathbf{M}\|[100]$ the global minimum has moved to $a=3.816$ Å and $c/a=0.994$. Contrary to LSDA, where no crossing between the two surfaces occurs, within GGA the two surfaces cross, thus producing two different magnetic phases with magnetization parallel or perpendicular to the substrate.

Figure 6 shows the perpendicular and parallel magnetization phases within GGA as a function of the lattice parameter a and the c/a ratio. This graph shows three magnetic regions separated by two transition lines. In the region between these two lines the MCA is negative favoring the [100] axis. On this figure we have added also the positions of the global minimum for both magnetization axis and the position of three experimental points. The first experimental point corresponds to the sample investigated by Le Can *et al.* and by

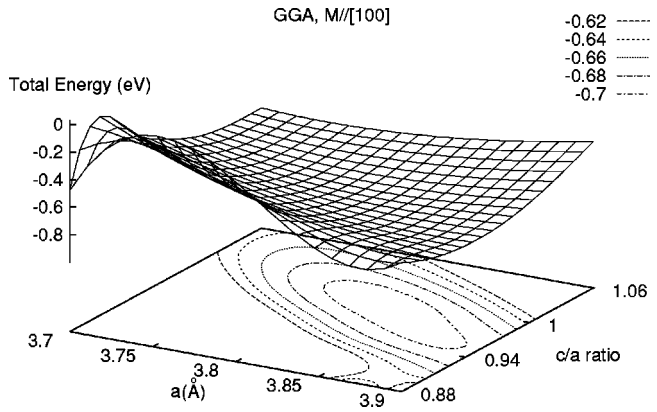

FIG. 5. The same as Fig. 4 but for $\mathbf{M}\|[100]$. The surface has the same form as for $\mathbf{M}\|[001]$ but the position of the global minima has changed and is now located at $a=3.816$ Å and $c/a=0.994$.

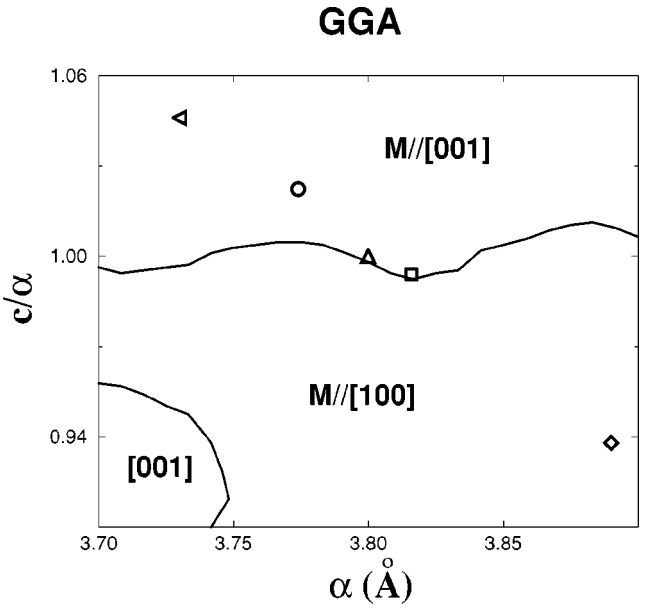

FIG. 6. The two lines limit the two different magnetic phases obtained as a function of the a and c/a lattice parameters within the GGA. The calculated minima for the two magnetization axes (the circle is for the [001] direction and the square is for the [100]), together with the FCC (up triangle), and the CFCT point (diamond) lattice parameters are presented. The last point (side triangle) corresponds to the EFCT sample. The phase with the magnetization axis along the [100] direction is obtained for large values of a and low c/a ratios and the [001] magnetization axis for the remaining values of a and c/a.

Boeglin *et al.*, which we define as an elongated face-centered tetragonal sample (EFCT) and has lattice parameters $a=3.73$ Å, $c=3.90$ Å ($c/a=1.046$);[8,9] the second point represents the disordered γ fcc lattice ($a=3.8$ Å), and is the ground state for the bulk $Fe_{0.5}Pd_{0.5}$ alloy (FCC);[5] and the third point corresponds to the Kamp's sample at 623 K which is highly ordered (91% of the atoms are in the correct sites) and we define as compressed face-centered tetragonal (CFCT) and with lattice parameters $a=3.89$ Å, $c=3.65$ Å and c/a ratio 0.938.[7] The FCC point is very close to the calculated minimum and very close to the zero isoline. CFCT point is inside the region with $\mathbf{M}\|[100]$ far from the zero isoline. Experimentally this point is found to have its magnetization axis along the [001] direction in agreement with our LSDA calculation but surprising is the discrepancy with our GGA predictions. Notice that our calculations are limited to calculating the total energy at zero temperature while the experimental results are obtained at 623 K. These thermal effects and shape anisotropy could easily switch between the two phases. In this respect, theoretical computation of MCA as a function of temperature is of great interest.

In Table I we present our calculated MCA for experimental lattice parameters and compare them with the experimental MCA values and with other theoretical data. These calculations have been converged up to 6750 k- points in the Brillouin zone.[31] It is surprising that MCA values within GGA are one order of magnitude larger than these obtained within LSDA. The only rational explanation for this behavior is that GGA strictly favors one magnetization axis over the other one. We should notice here that GGA is a relatively

TABLE I. Calculated LSDA and GGA magnetocrystalline anisotropy (MCA) for ordered $Fe_{0.5}Pd_{0.5}$ alloy. The MCA is defined as the difference in total energy between the two magnetization axis: $MCA = E_{tot}(M\|[100]) - E_{tot}(M\|[001])$. The GGA results are one order of magnitude larger than within the LSDA and for the CFCT it favors the [100] magnetization axis contrary to LSDA. For all the other cases our results favor the [001] magnetization axis. The experimental result is from Ref. 7.

MCA (meV)	EFCT	FCC	CFCT
LSDA	0.34	0.24	0.06
GGA	3.56	0.95	−0.34
Expt.			0.34

new functional and has not yet been much tested for the computation of MCA, consequently it does not represent an improvement over LSDA. From this point of view, its use instead of LSDA is not always justified and it is the comparison with experiment for each system and property that justifies the use of either LSDA or GGA. In the case of $Fe_{0.5}Pd_{0.5}$ LSDA seems to be adequate for the prediction of MCA.

The thin film elaborated by Boeglin *et al.* shows an in-plane axis contrary to our calculations for the EFCT. We should notice that there is no experimental measurement of the MCA for this film and that only the direction of the magnetization is reported on a disordered 4 ML sample which is expected to show noncollinear magnetism. The thick film corresponding to CFCT shows a magnetization along the [001] direction in agreement with LSDA. Kamp *et al.*[7] found for this film a value of 0.37 meV for the magnetic anisotropy energy (MAE), more important than LSDA result (0.06 meV). In particular, Daalderop *et al.*[10] used a unit cell of c/a ratio of 0.96 to compute the MCA within LSDA by means of the force theorem.[32] They found the magnetization along the [001] axis in agreement with our LSDA results and an MCA value of 0.51 meV, much larger than our value. This high MCA value is probably due to the use of the atomic sphere approximation (ASA) to the LMTO method.[33] More interestingly, they showed that the magnetoelastic anisotropy for this system is at least one order of magnitude smaller than MCA. Solovyev *et al.*[12] used the same structure within a real-space Green's function technique to find out that the magnetization is along the [001] axis. However, the MCA value was found to vary from 0.054 meV, when the spin-orbit coupling is treated as a pseudoperturbation taking into account only the *d* states, up to 0.29 meV, when the spin-orbit coupling for the *p* states is also included.[12] Here again the atomic sphere approximation is used.

To determine whether the bulk calculations are appropriate to describe the magnetic properties of the $Fe_{0.5}Pd_{0.5}$ films, we performed a supercell calculation of a 4 ML EFCT film. The memory requirements of our full-potential method limits the number of atoms per unit cell, so that we cannot account for the Pd(100) substrate in our supercell calculations. Both LSDA and GGA favor the [001] magnetization axis in agreement with the bulk calculations. The supercell calculated MCA is 0.18 meV/atom within LSDA and 2.14 meV/atom within GGA, which are comparable to the bulk calculations

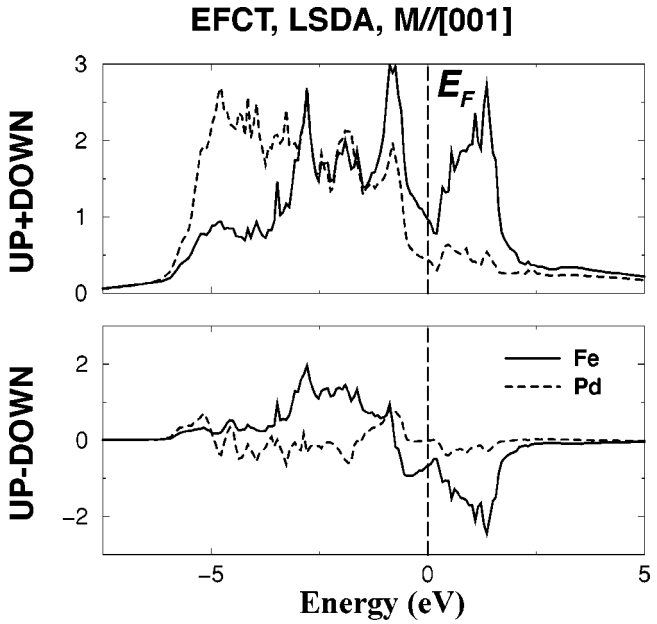

FIG. 7. Fe and Pd total density of states (upper panel) and spin resolved (lower panel). Pd has a broad complex typical for 4*d* metals in 3*d*-ferromagnet–4*d*-metal binary alloys. The Fe and Pd coupling is antiferromagnetic up to 1 eV below the Fermi level but the total one is ferromagnetic. Near Fermi level it is the spin down electrons of Fe that dominate the magnetic behavior of the alloy.

of 0.17 and 1.78 meV/atom, respectively. The discrepancy between our calculations and experiment for the 4 ML thin film should be attributed to the effect of the structure and of the chemical ordering that are not known for this sample. We should notice here that this film was produced by deposing two Fe layers on top of Pd(100). The interdiffusion of the Fe atoms on the Pd surface leads to the creation of a surface alloy, which is expected not to be ordered. Experimental lattice parameters were extracted by assuming the creation of a perfectly ordered 4 ML surface alloy and no further investigation was made.[9] Moreover, if the disorder is important we expect the magnetic state to be noncollinear.

III. MAGNETIC MOMENTS

In this section we discuss our calculated spin and orbital magnetic moments for the three sets of lattice parameters corresponding to the EFCT, FCC, and CFCT samples. The calculated density of states (DOS) for these three lattice parameters, are dominated by their *d* orbital contributions. So the discussion below refers primarily to the *d* part of the various DOS curves. The behavior of the DOS is insensitive to the exchange-correlation potential and the magnetization axis or the sample. The total density of states (upper panel Fig. 7) has the typical behavior of a binary 3*d*-ferromagnet–4*d*-metal alloy DOS. The Fe component dominates in the vicinity of the Fermi level, while the Pd shows a broad complex *d* band. The differences in DOS between the spin-up and spin-down resolved DOS (bottom panel of Fig. 7) show the coupling between Fe and Pd as antiferromagnetic for energies up to 1 eV below the Fermi level. The coupling becomes ferromagnetic for the total DOS. It is interesting to notice that in the vicinity of the Fermi level the Pd spin

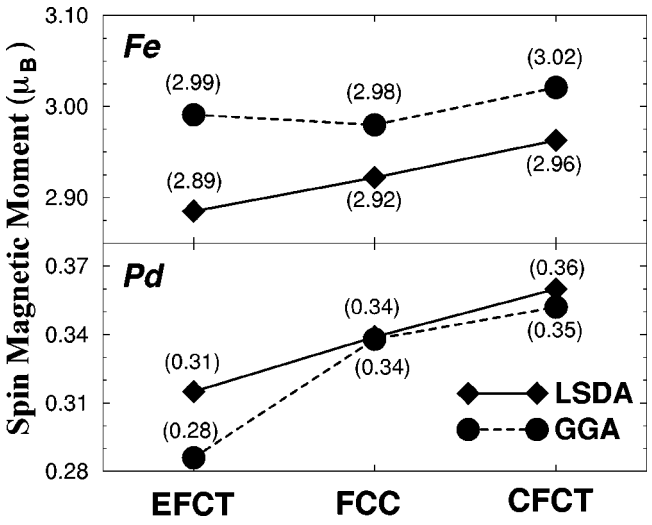

FIG. 8. LSDA and GGA spin magnetic moments of Fe and Pd. GGA produces a more atomiclike description of the band structure of $Fe_{0.5}Pd_{0.5}$ producing higher Fe magnetic moments compared to LSDA. The spin magnetic moments of Pd are induced by hybridization. As Fe becomes more atomiclike within GGA, the hybridization decreases resulting in a smaller Pd magnetic moment. The spin moments are insensitive to the magnetization direction.

imbalance is practically zero while for Fe the spin down states dominate.

Figure 8 shows the calculated spin magnetic moments of Fe and Pd sites calculated for the EFCT, FCC, and CFCT lattice parameters. They are found to be independent of the direction of the magnetization axis. The fact that GGA is known to produce a very atomiclike description of the solid is reflected on larger magnetic moments of the Fe sites compared to LSDA values. The overestimation of the Fe atomic character within GGA produces a much lower hybridization between Fe-3*d* and Pd-4*d* orbitals. Since Pd is paramagnetic, its magnetic moment is primarily due to hybridization with Fe. So a reduction in the hybridization amounts to a smaller induced spin-magnetic moments for Pd within GGA. Our calculated spin moments compare nicely with previous calculations. In particular, Moruzzi and Marcus[11] performed calculations for a perfect fcc lattice and found a spin magnetic moment of $2.9\mu_B$ for Fe and $0.4\mu_B$ for Pd. Experimentally, Cros *et al.*[34] performed XMCD measurements on the $L_{2,3}$ edges of Pd in $Fe_{0.5}Pd_{0.5}$ multilayers and applied the sum rules to find a spin magnetic moment of $0.4\mu_B$ for Pd in agreement with our results. However, Kamp found that the moments on Fe atoms in various films can vary from $2.04 \pm 0.05\mu_B$ in ordered samples up to $2.13 \pm 0.05\mu_B$ for the disordered ones.[7] These latter values are significantly lower than the calculated values and it is surprising that the magnetic moment for the disordered sample is higher than for the ordered one.

The spin magnetic moments for the 4 ML system are close to the values for the bulk calculations as can be seen in Table II especially for the Pd and Fe atoms that have the same first neighbors as in the bulk [Pd(1) and Fe(2) atoms]. Pd spin moments are insensitive to the exchange-correlation potential used. The induced moment of the outer Pd(2), that has only one Fe layer as neighbor, is smaller than that of Pd(1) which has two Fe layers. From this comparison we deduce that the magnetic properties of this alloy seem to be practically insensitive to the thickness of the film but depend strongly on the lattice parameters.

TABLE II. Spin magnetic moments for the 4 monolayer EFCT $Fe_{0.5}Pd_{0.5}$ calculated using a supercell geometry together with the EFCT bulk ones (inside parentheses). The calculated values are close to the bulk values and especially Pd moments are insensitive to the type of exchange-correlation potential used. The induced moment on the outer Pd(2) that has fewer Fe neighbors is smaller than for the inner Pd(1) that has two Fe layers as neighbors. The spin moments are isotropic with respect to the magnetization axis.

$m^{spin}(\mu_B)$	Fe(1)	Pd(1)	Fe(2)	Pd(2)
LSDA	3.01 (2.88)	0.31 (0.31)	2.95 (2.88)	0.26 (0.31)
GGA	3.04 (2.99)	0.31 (0.28)	3.01 (2.99)	0.26 (0.28)

Figure 9 shows that, contrary to the spin magnetic moments, the Fe and Pd sites orbital moments are not isotropic with respect to the magnetization axis. Here the LSDA orbital moments for Fe are much larger than the GGA values contrary to the spin moments. We observe also that the orbital moments calculated for the [001] magnetization axis are larger than the values for the in-plane [100] axis. Notice that the values of the orbital moments are just the projections of the total orbital moments on the spin-quantization axis and that we have no information concerning the direction and the total value of the orbital moments. Pd shows exactly an opposite behavior to Fe. The GGA values lay higher than these of the LSDA and the values for the [001] axis lay lower than for the [100] axis. The orbital moments on Fe sites are 3 times larger than for Pd sites, contrary to the spin moments where the difference was one order of magnitude. This is because orbital moments are not only induced by the spin-orbit coupling but also by the crystal field that breaks the

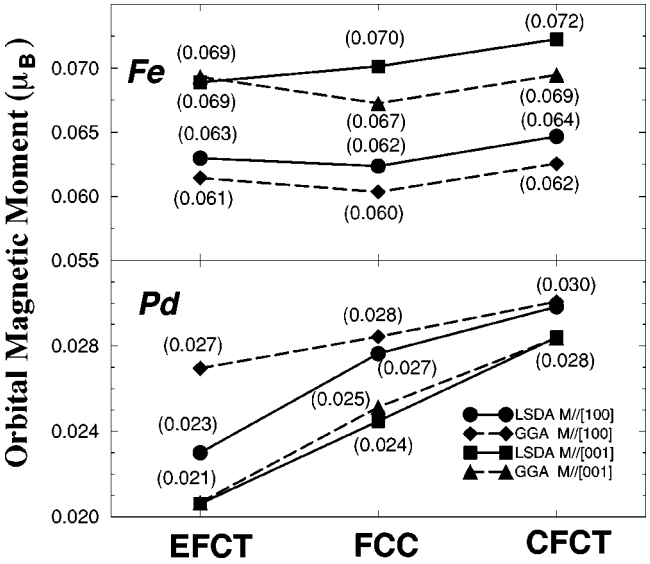

FIG. 9. LSDA and GGA orbital magnetic moments for both [001] and [100] magnetization axis. Fe orbital moments for the [001] axis are higher than for the [100] axis and LSDA gives higher values. For Pd side the behavior is exactly the contrary to the Fe site. Notice that the orbital moments are not isotropic with respect to the magnetization axis.

TABLE III. Orbital magnetic moments within LSDA for magnetization along the [001] axis. The inclusion of the orbital polarization term (Ref. 35) scarcely changes the results contrary to bulk bcc Fe where orbital magnetic moment increases by 70%.

$m^{\text{orbital}}(\mu_B)$		EFCT	FCC	CFCT
Fe	LSDA	0.069	0.070	0.072
	LSDA+OP	0.069	0.071	0.073
Pd	LSDA	0.021	0.024	0.028
	LSDA+OP	0.020	0.023	0.026

symmetry. Cros *et al.*[34] applied the sum rules and obtained an orbital moment of $0.004\mu_B$ for Pd site, about one order of magnitude smaller than our calculated values. But because the error on the values of the orbital moment obtained from the sum rules exceeds easily $0.01\mu_B$, we believe that our result is in qualitative agreement with experiment.[20] No information for the experimental sample is available but probably the discrepancy comes from the effect of the disorder in the sample and from the limited applicability of the sum rules to the $4d$ system. Regarding the Fe site orbital moments, Kamp found it to vary from $0.42\pm0.05\mu_B$ in the ordered sample down to $0.22\pm0.05\mu_B$ for the disordered alloy,[7] much higher than the calculated values. These experimental values are about five times larger than the values for the bulk bcc Fe. This difference is surprisingly large inspite that the orbital moment is primary an atomic property. It is well know that both LSDA and GGA underestimate the orbital moments,[35] however, they usually produce the correct trend as a function of the lattice parameter or the magnetization direction.[40]

To improve our orbital moment results we included an orbital-polarization (OP) correction to the LSDA Hamiltonian. This additional term to the Hamiltonian was derived by Brooks[35] from an atomic theory but its use in the case of itinerant electrons is not always sufficient to describe electronic orbital moments. Table III shows the orbital magnetic moments for all the three structures within LSDA and for the magnetization axis along the [001] direction both with and without the orbital polarization term. Our calculation shows that this OP term slightly increases the Fe orbital moments and slightly decreases the Pd ones. Thus the OP term seems to be unimportant for $Fe_{0.5}Pd_{0.5}$ alloy contrary to bulk Fe where the inclusion of the OP increases the orbital magnetic moment from $0.050\mu_B$ to $0.085\mu_B$ improving considerably the agreement with experiment. These results show that the failure of LSDA to treat exactly the orbital magnetism can not always be improved by adding an OP term and that one should also improve the exchange-correlation interaction as well. The later correction is described by the current and spin density functional theory (CSDFT),[36] which treats the Kohn-Sham and the Maxwell equations in the same footing, however this formalism is complicated and computationally involved to be implemented as an *ab initio* method. Rajagopal[37] expanded this approach to include relativistic effects and recently Grayce and Harris[38] suggested a magnetic density functional theory as an alternative to CSDFT but it seems that no successful parametrization for none of these new approaches is available yet.[39]

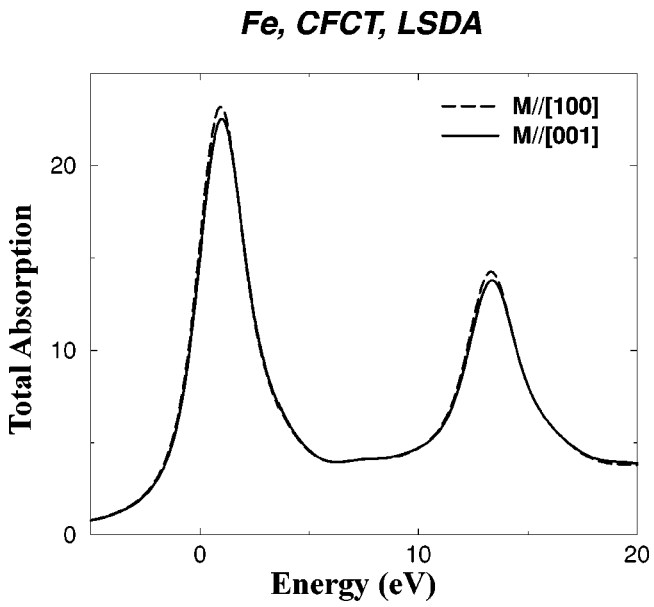

FIG. 10. Total absorption spectra for Fe within LSDA. The intensity is insensitive to the magnetization direction. The spin-orbit splitting for the $2p$ core states is 12.5 eV.

IV. XMCD

The last part of our work concerns the investigation of the behavior of XMCD of the $L_{2,3}$ edges of both Fe and Pd sites. We performed calculations using both LSDA and GGA and for both magnetization axis (i) $\mathbf{M}\|[001]$ and (ii) $\mathbf{M}\|[100]$. Experimentally the XMCD spectra have been measured by Kamp *et al.*[7] at the Fe $L_{2,3}$ edges for thick (300 Å) films and by Le Can *et al.* for thin films [2 monolayers of Fe on Pd(100)].[8]

A. Fe site

Figure 10 shows the LSDA calculated total absorption spectra corresponding to the CFCT sample, for the two magnetization axes. For the broadening of the theoretical spectra we used a Gaussian width of 0.4 eV and a Lorentzian width of 0.9 eV corresponding to the core-hole effect and to experimental resolution respectively. These values were used by Ebert in the case of Fe,[21] and by Alouani *et al.* for Fe in Fe nitrides.[22] Although different broadenings change the intensities of the peaks, they leave unchanged the L_3/L_2 integrated branching ratio, which is the most important feature of these spectra as it enters the sum rules. The absorption spectra are found to be insensitive to the type of exchange-correlation potential used, and depend only on the magnetization axis. We notice that for $\mathbf{M}\|[100]$ the intensity for both L_2 and L_3 peaks are larger than for $\mathbf{M}\|[001]$. The energy difference between the L_2 and L_3 peaks is given by the spin-orbit splitting between the $p_{1/2}$ and $p_{3/2}$ core states. The theoretical value is 12.5 eV and is very close to the experimental 12.4 eV value of bulk Fe. Since the core states are not considerably affected by the crystalline environment of Fe, it is then expected that the spin-orbit splitting remains practically unchanged in different Fe alloys.

Figure 11 shows the calculated XMCD spectra within LSDA for lattice parameters corresponding to the three samples and for the two magnetization axes. The L_3/L_2 in-

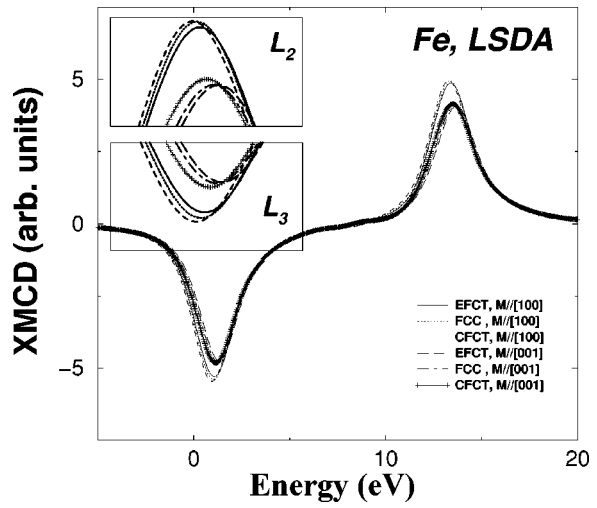

FIG. 11. XMCD spectra for Fe within LSDA for different magnetization axis and for the three chosen structures. L_3/L_2 integrated branching ratio is independent from the structure itself. In-plane spectra and compressed structure lay higher in intensity for both peaks. GGA produces results similar to LSDA.

tegrated branching ratio depends only on the magnetization axis and is larger in the case of $\mathbf{M}\|[100]$. The CFCT higher intensities, as compared to the FCC and the EFCT, implies that the intensities of the two peaks depend primarily on the value of the lattice parameter *a*, and it increases as *a* increases. Both L_2 and L_3 peaks show the same behavior as it can be seen in the two small graphs, where we have enlarged the area around the two peaks. The calculated number of holes in the *d*-bands are 3.79 and 1.91 for Fe and Pd, respectively.

Figure 12 compares our $L_{2,3}$ XMCD result for Fe site, within LSDA and for $\mathrm{M}\|[001]$ using the lattice parameters of the EFCT sample, with the experimental results of Le Can *et al.*[8] We calculated the XMCD spectrum for both the bulk and the 4 monolayer system. We have normalized the theoretical spectrum so that the calculated L_3 peak has the same intensity as that of the experimental spectrum. The theory underestimates the L_3/L_2 ratio by about 50% (2.70 for experiment, 1.14 for the bulk calculation). Part of the discrepancy between experiment and theory comes from the fact that we performed calculations for a bulk alloy while experiment was performed for a *thin film* (4ML of surface alloy). However, the supercell calculation for the 4 monolayer film scarcely improves the agreement between theory and experiment ($L_3/L_2=1.19$). This supercell represents a free-standing film and does not account for the influence of the Pd(100) substrate to determine the electronic structure of the film. The agreement between the theory and experiment can be improved by taking into account the photoexcited electron core-hole interaction.[22] A formalism that can account for this interaction has been proposed by Schwitalla and Ebert,[41] however, the formalism is computationally heavy and the results are not satisfactory. Benedict and Shirley[42] have also developed a scheme to treat this interaction but it is limited to crystalline insulators.

In Fig. 13 we present also $L_{2,3}$ XMCD results obtained for the lattice parameters of CFCT structure. Our calculated branching ratio is much closer than in the case of EFCT

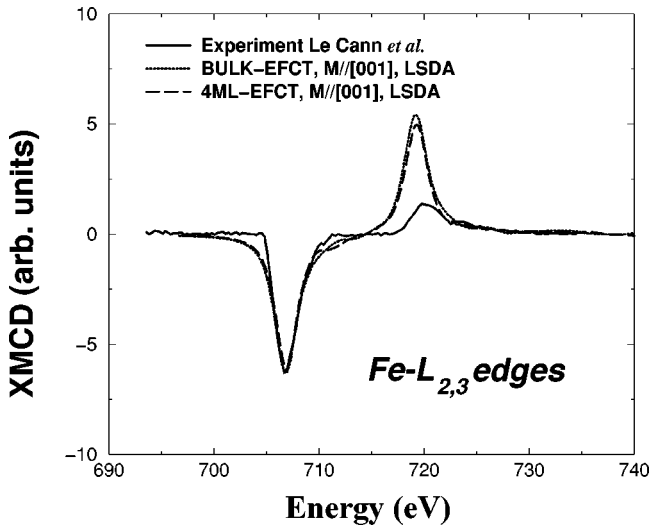

FIG. 12. Bulk and supercell calculated XMCD spectrum for the $L_{2,3}$Fe edge of expanded fct $Fe_{0.5}Pd_{0.5}$ alloy compared to the experimental thin film spectrum of 4 monolayers $Fe_{0.5}Pd_{0.5}$ surface alloy on a Pd(100) substrate (Ref. 8). The integrated L_3/L_2 branching ratio is underestimated by our calculations ($L_3/L_2=2.70$ in experiment and 1.14 for the bulk calculation and 1.19 for the supercell one). This underestimation is pronounced by the comparison between a bulk calculation and a very thin supported film. The supercell calculation for the free 4 monolayer film fails to reproduce the properties of the supported thin film.

(1.32 for experiment and 1.12 for theory). The CFCT sample is a 300 Å thick film,[7] so it approaches more the bulk system which was not the case for the EFCT sample. Discrepancy comes from the partial disorder of the experimental film and from the neglect of the photoexcited electron core-hole interaction in the calculations. It is worth mentioning that the radiation used in the experiments is only $\sim$ 90% circularly

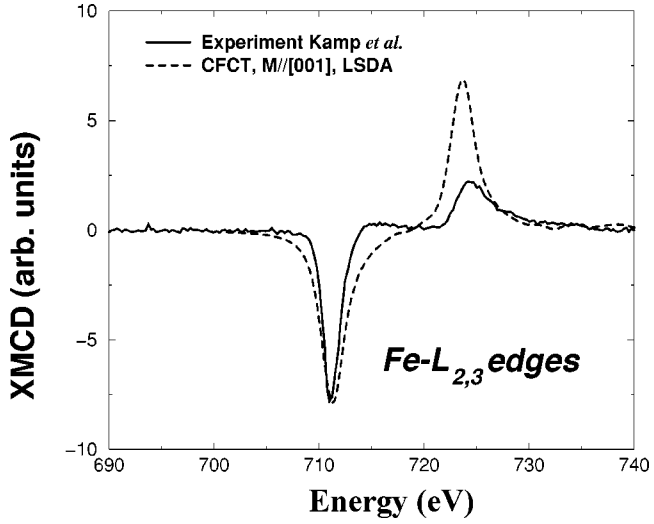

FIG. 13. Theoretical XMCD spectrum for $L_{2,3}$Fe edge of compressed fct $Fe_{0.5}Pd_{0.5}$ alloy compared to experimental thick film deposited on MgO(001) at 623K by molecular beam epitaxy (Ref. 7). The L_3/L_2 integrated branching ratio is underestimated by our theory but the calculated and experimental values are much closer than in the case of EFCT (1.32 for experiment compared to 1.12 for theory).

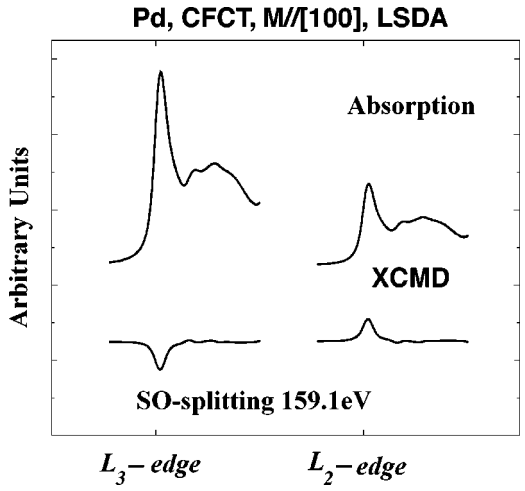

FIG. 14. L_2 and L_3 absorption and XMCD spectra for Pd within LSDA for the [100] magnetization axis. The spin-orbit energy difference between the two peaks is 159.1 eV close to the experimental value of 160 eV. The total absorption spectra is insensitive to the magnetization axis.

polarized, and the rest are linearly polarized. Even if the experimental graphs are scaled to account for 100% circular polarization, they ignore the contribution of the x-ray magnetic linear dichroism (XMLD). Furthermore XMLD signal is much weaker compared to that of the XMCD, so it should not influence significantly the experimental spectrum.

B. Pd site

In Fig. 14 we present results within LSDA for the CFCT system and for magnetization along the [100] axis for the Pd site. The spin-orbit splitting energy of the $2p$ states of Pd is one order of magnitude larger than for the Fe site (159.1 eV compared to 13.5 eV) and compares nicely with the experimental value of 160 eV.[7] This large value allows the independent measurement of the L_2 and L_3 edges. We observe that the absorption peak for the L_3 edge is more important than that of the L_2 edge. XMCD spectra are also presented in the same figure. Contrary to Fe, LSDA and GGA give different spectra but the branching ratio does not change with the way we treat the exchange-correlation potential. In Fig. 15 we present the L_2 edge for M∥[001] within both LSDA and GGA and for the three structures. Results are exactly equivalent for the L_3 edge and hence are not presented. LSDA produces in all cases higher intensities than GGA, and especially for the EFCT system the difference is quite important. As in the case of Fe as the lattice parameter a increases the intensities of absorption increase accordingly. In the next figure (Fig. 16) we present the same edge within LSDA but for both magnetization axis; the results are similar in the case of GGA. As in the case of Fe, when **M**∥[100] the intensities of the peak is more important than when **M**∥[001]. The branching ratio still depends primarily on the magnetization axis.

V. CONCLUSION

We have investigated the magnetic properties of the $Fe_{0.5}Pd_{0.5}$ ordered face-centered tetragonal alloy under strain

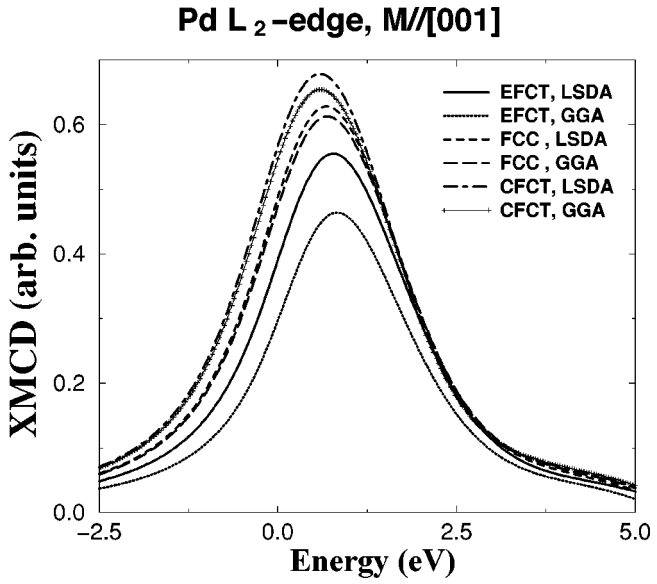

FIG. 15. XMCD spectra for the L_2 edge of Pd and for **M**//[001]. The trends for the L_3 are exactly the same. The LSDA gives higher intensities than the GGA, but the branching ratio does not change with the exchange-correlation potential. The intensities increase with the decreasing c/a ratio.

in terms of an *ab initio* relativistic full-potential LMTO method. The total energy with respect to the lattice parameters a and c/a shows a valley along an isovolume line which could lead to stable structures within this valley. Such a structure could exist due to lattice mismatch between the $Fe_{0.5}Pd_{0.5}$ film and the substrate. We predicted a spin magnetic transition within the generalized gradient approximation (GGA), due to the crossing of the **M**∥[100] total energy surface with that of **M**∥[001] direction, but not within the local spin density approximation (LSDA). In fact LSDA fa-

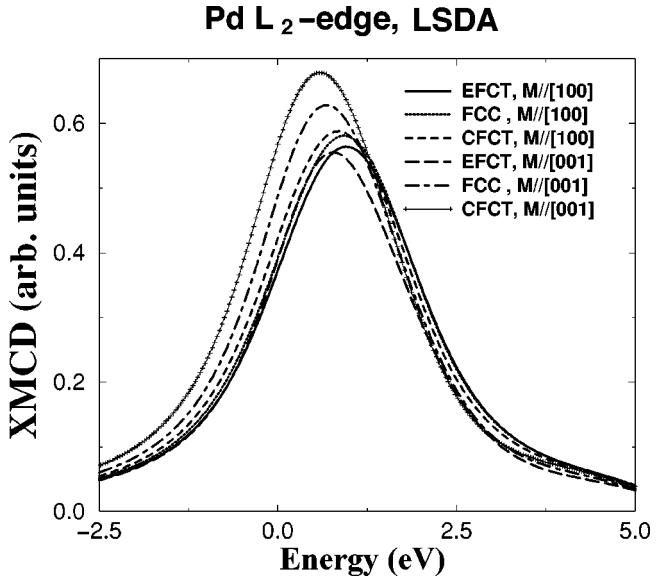

FIG. 16. XMCD spectra for the L_2 edge of Pd calculated within LSDA. The trends for the L_3 are exactly the same. The [001] axis give higher intensities than the in-plane one. The intensities increase with decreasing c/a ratio. The branching ratio is sensitive to the magnetization axis.

vored the [001] magnetization direction for all the values of the lattice parameters. It is too early to decide whether the results of GGA are superior to these of LSDA because GGA is a relatively new functional and has not been tested thoroughly for the computation of the magnetocrystalline anisotropy energy (MCA). More testing should be done before deciding whether GGA is appropriate for the calculation of such a sensitive property. For the 300 Å thick film LSDA produced the correct magnetization axis while GGA did not. As for the 4 monolayer (ML) $Fe_{0.5}Pd_{0.5}$ thin film both LSDA and GGA failed to produce the correct direction of the magnetization. However, we should notice that there is no experimental measurement of the MCA and that only the direction of the magnetization is reported on a disordered 4 ML sample which is expected to show noncollinear magnetism. Therefore an experimental determination of the MCA is necessary before drawing any conclusion regarding the MCA of the $Fe_{0.5}Pd_{0.5}$ films.

We found that GGA produces a more atomiclike description of the electronic structure as compared to LSDA and this behavior is reflected on larger magnetic moments of Fe site within GGA and the reduction of the Pd induced magnetic moment which is essentially due to hybridization between Fe-3*d* orbitals and Pd-5*d* orbitals. The inclusion of the orbital polarization term does not change considerably the calculated orbital magnetic moments.

X-ray magnetic circular dichroism (XMCD) spectra are calculated within GGA and LSDA for two magnetization axes and for three sets of lattice parameters. Fe site computed XMCD spectra are compared to experiments and as in the case of bulk Fe the integrated L_3/L_2 branching ratio is underestimated. A 4 monolayer supercell calculation produced results in agreement with our bulk calculations suggesting that the bulk description of the $Fe_{0.5}Pd_{0.5}$ films is appropriate. An improvement of the integrated L_3/L_2 branching ratio could be achieved by including the photoelectron core-hole interaction, the temperature, and the disorder effects. These contributions are not possible within our $T=0$ K *ab initio* method and are therefore beyond our capabilities.

ACKNOWLEDGMENTS

The authors are indebted to Christine Boeglin for her interest in our work and for helpful discussions. One of us (S.O.) acknowledges financial support from a grant by ''Le Ministere de l'Education Nationale, de la Recherche et de la Technologie'' of France. Supercomputer time was granted by CNUSC (project gem1917) on the IBM SP2 and by the Université Louis Pasteur de Strasbourg on the SGI O2000 supercomputer. I.G. was supported by the EU (Grant No. ERBFMXCT96-0089).

[1] B. M. Lairson and B. M. Clemens, Appl. Phys. Lett. **63**, 1438 (1993).

[2] I. Osterloch, P. M. Oppeneer, J. Sticht, and J. Kübler, J. Phys.: Condens. Matter **6**, 285 (1994).

[3] V. Gehanno, A. Marty, B. Gilles, and Y. Samson, Phys. Rev. B **55**, 12 552 (1997); V. Gehanno, Ph.D. thesis, INPG, Grenoble, 1997; V. Gehanno, Y. Samson, A. Marty, B. Gilles, and A. Chamberod, J. Magn. Magn. Mater. **172**, 26 (1997); V. Gehanno, C. Revenant-Brizard, A. Marty, and B. Gilles, J. Appl. Phys. **84**, 2316 (1998).

[4] A. Kussmann and K. Müller, Z. Angew. Phys. **17**, 509 (1964); L. M. Magat, A. S. Yermolenko, G. V. Ivanova, G. M. Makarova, and Ya S. Shur, Fiz. Met. Metalloved. **26**, 511 (1968); V. V. Mayokov, A. Ye Yermakov, G. V. Ivanov, V. I. Khrabrov, and L. M. Magat, *ibid.* **67**, 79 (1989); A. Ye Yermakov and V. V. Mayokov, *ibid.* **69**, 198 (1990).

[5] F. C. Nix and W. Shockley, Rev. Mod. Phys. **10**, 1 (1938).

[6] H. Okumura, W. A. Soffa, T. J. Klemmer, and J. A. Barnard, IEEE Trans. Magn. **34**, 1015 (1998).

[7] P. Kamp, A. Marty, B. Gilles, R. Hoffmann, S. Marchesini, M. Belakhovsky, C. Boeglin, H. A. Dürr, S. S. Dhesi, G. van der Laan, and A. Rogalev, Phys. Rev. B **59**, 1105 (1999).

[8] X. Le Cann, C. Boeglin, B. Carrière, and K. Hricovini, Phys. Rev. B **54**, 373 (1996).

[9] C. Boeglin, H. Bulou, J. Hommet, X. Le Cann, H. Magnan, P. Le Fèvre, and D. Chandesris, Phys. Rev. B **60**, 4220 (1999).

[10] G. H. O. Daalderop, P. J. Kelly, and M. F. H. Shuurmans, Phys. Rev. B **44**, 12 054 (1991).

[11] V. L. Moruzzi and P. M. Marcus, Phys. Rev. B **48**, 16 106 (1993).

[12] I. V. Solovyev, P. H. Dederichs, and I. Mertig, Phys. Rev. B **52**, 13 419 (1995).

[13] D. Weller, J. Stöhr, R. Nakajima, A. Carl, M. G. Samant, C. Chappert, R. Mégy, P. Beauvillain, P. Veillet, and G. A. Held, Phys. Rev. Lett. **75**, 3752 (1995).

[14] *Spin-orbit Influenced Spectroscopies of Magnetic Solids*, Vol. 466 of *Lecture Notes in Physics*, edited by H. Ebert and G. Schütz (Springer-Verlag, Heidelberg, 1996).

[15] B. T. Thole, P. Carra, F. Sette, and G. van der Laan, Phys. Rev. Lett. **68**, 1943 (1992).

[16] P. Carra, B. T. Thole, M. Altarelli, and X. Wang, Phys. Rev. Lett. **70**, 694 (1993).

[17] G. van der Laan, Phys. Rev. B **57**, 112 (1998).

[18] C. T. Chen, Y. U. Idzerda, H.-J. Lin, N. V. Smith, G. Meigs, E. Chaban, G. H. Ho, E. Pellegrin, and F. Sette, Phys. Rev. Lett. **75**, 152 (1995).

[19] Notice that the magnetic dipole term can represent a significant contribution to the effective spin magnetic moment [up to 50% at the (001) surface of Ni] (see Ref. 20).

[20] R. Wu, D. Wang, and A. J. Freeman, Phys. Rev. Lett. **71**, 3581 (1993); R. Wu and A. J. Freeman, *ibid.* **73**, 1994 (1994).

[21] H. Ebert, Rep. Prog. Phys. **59**, 1665 (1996).

[22] M. Alouani, J. M. Wills, and J. M. Wilkins, Phys. Rev. B **57**, 9502 (1998).

[23] C. Brouder and M. Hikam, Phys. Rev. B **43**, 3809 (1991); Ch. Brouder, M. Alouani, and K. H. Bennamann, *ibid.* **54**, 7334 (1996).

[24] G. Y. Guo, Phys. Rev. B **57**, 10 295 (1998).

[25] A. Ankudinov and J. J. Rehr, Phys. Rev. B **56**, 1712 (1997).

[26] G. van der Laan and B. T. Thole, Phys. Rev. B **43**, 13 401 (1991).

[27] J. M. Wills and B. R. Cooper, Phys. Rev. B **36**, 3809 (1987); M. Alouani and J. M. Wills, *ibid.* **54**, 2480 (1996).

[28] P. Hohenberg and W. Kohn, Phys. Rev. B **136**, A864 (1964); W.

Kohn and L. J. Sham, Phys. Rev. **140**, A1133 (1965).
[29] U. von Barth and L. Hedin, J. Phys. C **5**, 1629 (1972).
[30] J. P. Perdew and Y. Wang, Phys. Rev. B **33**, 8800 (1986); **45**, 13 244 (1992).
[31] We have found that this value of k points is sufficient because differences in the MCA values calculated for 1458 and 6750 k points are less than 1%.
[32] A. R. Macintosh and O. K. Andersen, in *Electrons at the Fermi Surface*, edited by M. Springfold (Cambridge University Press, Cambridge, 1980).
[33] O. K. Andersen, Phys. Rev. B **12**, 3060 (1975).
[34] V. Cros, F. Petroff, J. Vogel, A. Fontaine, J.-P. Kappler, G. Krill, A. Rogalev, and J. Goulon, J. Appl. Phys. **81**, 3774 (1997).
[35] M. S. S. Brooks, Physica B **130**, 6 (1985).
[36] G. Vignale and M. Resolt, Phys. Rev. B **37**, 10 685 (1988).
[37] A. K. Rajagopal, Phys. Rev. A **50**, 3759 (1994).
[38] C. J. Grayce and R. A. Harris, Phys. Rev. A **50**, 3089 (1994).
[39] G. Vignale, in *Current Density Functional Theory and Orbital Magnetism*, Vol. 337 of *NATO Advanced Study Institute, Series B: Physics*, edited by E. K. U. Gross and R. M. Dreizler (Plenum Press, New York, 1995), p. 485.
[40] W. Grange, I. Galanakis, M. Alouani, M. Maret, Kappler, and A. Rogalev, Phys. Rev. B (to be published).
[41] J. Schwitalla and H. Ebert, Phys. Rev. Lett. **80**, 4586 (1998).
[42] L. X. Benedict and E. L. Shirley, Phys. Rev. B **59**, 5441 (1999).